

# On the instability of buoyancy-driven flows in porous media

Shyam Sunder Gopalakrishnan<sup>1,2,†</sup>

<sup>1</sup>Nonlinear Physical Chemistry Unit, Université Libre de Bruxelles (ULB), CP231,  
1050 Brussels, Belgium

<sup>2</sup>Physique des Systèmes Dynamique, Université Libre de Bruxelles (ULB), CP231,  
1050 Brussels, Belgium

(Received 25 July 2019; revised 4 February 2020; accepted 10 March 2020)

The interface between two miscible solutions in porous media and Hele-Shaw cells (two glass plates separated by a thin gap) in a gravity field can destabilise due to buoyancy-driven and double-diffusive effects. In this paper the conditions for instability to arise are presented within an analytical framework by considering the eigenvalue problem based on the tools used extensively by Chandrasekhar. The model considered here is Darcy's law coupled to evolution equations for the concentrations of different solutes. We have shown that, when there is an interval in the spatial domain where the first derivative of the base-state density profile is negative, the flows are unstable to stationary or oscillatory modes. Whereas for base-state density profiles that are strictly monotonically increasing downwards such that the first derivative of the base-state density profile is positive throughout the domain (for instance, when a lighter solution containing a species A overlies a denser solution containing another species B), a necessary and sufficient condition for instability is the presence of a point on either side of the initial interface where the second derivative of the base-state density profile is zero such that it changes sign. In such regimes the instability arises as non-oscillatory modes (real eigenvalues). The neutral stability curve, which delimits the stable from the unstable regime, that follows from the discussion presented here along with the other results are in agreement with earlier observations made using numerical computations. The analytical approach adopted in this work could be extended to other instabilities arising in porous media.

**Key words:** buoyancy-driven instability, convection in porous media

---

## 1. Introduction

The onset of instability of a horizontal interface separating two miscible solutions in a porous medium has been the subject of investigation in a number of theoretical and experimental studies. The problem finds application in several fields of natural science due to its direct relevance in innumerable industrial applications, such as surface and colloid physical chemistry, soil physics, petroleum engineering and powder metallurgy,

† Email address for correspondence: [shyam7sunder@gmail.com](mailto:shyam7sunder@gmail.com)

in addition to its academic interest from a fluid mechanics point of view regarding the evolution of instabilities and the subsequent nonlinear dynamics (Philip 1970; Huppert & Sparks 1984; Homsy 1987; Schmitt 1994; Schmitt *et al.* 2005; Trevelyan, Almarcha & De Wit 2011; Huppert & Neufeld 2014).

The conditions for the interface between two immiscible fluids with different densities and viscosities in a porous medium to destabilise and deform into finger-like structures when subject to a gravitational field or an imposed pressure gradient were laid out by Saffman & Taylor (1958). This followed from the well-known Rayleigh–Taylor (RT) instability that occurs when a denser solution overlies a lighter one, which deforms the interface between them (Manickam & Homsy 1995; Fernandez *et al.* 2001, 2002; Martin, Rakotomala & Salin 2002; Gandhi & Trevelyan 2014; Gopalakrishnan *et al.* 2017; De Paoli, Zonta & Soldati 2019*b*).

In an initially statically stable system with a less dense solution overlying a denser solution, the miscible interface separating the two solutions can destabilise due to differential diffusion of solutes, where the driving energy comes from the component having the higher or lower diffusivity. When the solute in the denser lower solution diffuses faster than the solute in the lighter upper solution, a double-diffusive (DD) instability develops, which triggers a convective motion deforming the interface into fingers that develop symmetrically across it (Turner 1979; Huppert & Turner 1981; Green 1984; Huppert & Sparks 1984; Schmitt 1994; Cooper, Glass & Tyler 1997; Pringle & Glass 2002; Schmitt *et al.* 2005; Trevelyan *et al.* 2011; Radko 2013). Apart from the differential diffusion of solutes such as salt and sugar (for instance), which result in double diffusion (Pringle & Glass 2002), such phenomena are responsible for the thermohaline convection observed in oceans, which is triggered due to the differential diffusion of salt and heat (Schmitt 1994; Schmitt *et al.* 2005).

Instability also arises when the solute in the lighter upper solution diffuses faster than the one in the lower denser solution. Regions with locally unstable density gradients develop over time induced by a differential diffusion effect, and is termed as diffusive-layer convection (DLC) (Turner & Stommel 1964; Griffiths 1981; Turner 1985; Trevelyan *et al.* 2011). The faster diffusion of the upper solute towards the denser lower solution results in a depletion zone above the interface, and an accumulation below, triggering a convective motion on either side of the initial interface.

In all the scenarios presented so far, the differential diffusion of the solutes can lead to non-monotonic density profiles, which significantly influence the flow dynamics (Trevelyan *et al.* 2011; Carballido-Landeira *et al.* 2013; Gopalakrishnan *et al.* 2018). The RT instability involving a single species seldom occurs in the various porous media flows observed in nature and in industrial processes, as double-diffusive effects usually coexist, due to the difference in the differential diffusion of solutes. This coupling between diffusive and convective processes can result in a double-diffusive flux that could be much larger than in a single solutal system (Turner 1985).

The stability, or the instability, of these buoyancy-driven flows has been mainly addressed using linear base states for the time-evolving density profiles, or by means of numerical linear stability analyses. In the context of DD instabilities, the limiting conditions for salt fingering to occur at an interface were provided by Huppert & Sparks (1984) by considering linear base states. They showed that an infinitesimal perturbation will develop into fingers when  $R < \tau^{3/2}$ , where  $R$  is the buoyancy ratio and  $\tau$  is the diffusion coefficient ratio (that of heat to that of salt, in this instance). The buoyancy ratio  $R$  expresses the relative solutal buoyancy contribution of each species to the density profile. Trevelyan *et al.* (2011) carried out a stability

analysis of various buoyancy-driven flows in a two-dimensional porous medium and Hele-Shaw cells. Using a quasi-steady-state approximation, they carried out a linear stability analysis of time-evolving base-state profiles numerically and mapped out the various regimes of instability in the  $(R, \tau)$  parameter space. The neutral stability curve obtained numerically was in agreement with that of Huppert & Sparks (1984). More recently, using analytical methods, the onset conditions for an RT instability to develop were investigated by Gandhi & Trevelyan (2014), where they used a linear combination of step functions for the base-state concentration profiles.

In the present work we provide analytically the conditions for instability to develop in the various aforementioned buoyancy-driven flows in porous media. Specifically, we address ourselves to this problem and ask: Can we predict whether the interface separating two miscible solutions inside a vertically oriented two-dimensional porous medium or a Hele-Shaw cell is stable, or unstable, from the base-state density profile of the concentrations? Or, alternatively, can we provide the conditions for instability in these flows?

The analytical approach adopted in the present work has been previously used in the context of Rayleigh–Bénard convection, instability of shear layers and Taylor–Couette flows, among other hydrodynamic instabilities (Roberts 1960; Chandrasekhar 1961). Unlike in the earlier analytical works, where linear base states were considered, we have used time-evolving base-state profiles to extract information regarding the stability of the system. For instance, in the parameter space corresponding to  $\tau > 1$  and  $R > 1$ , Trevelyan *et al.* (2011) numerically found that the maximum growth rates were always real, which is confirmed in this study. Specifically, when the base-state density profiles are strictly monotonically increasing downwards, such that the density gradient of the base state is positive, we have shown that instability develops if and only if the second derivative of the base-state density profile is zero at a point on either side of the initial interface such that it changes sign. In these regimes, instability arises as stationary modes, with real eigenvalues. Whereas, when there is an interval in the spatial domain where the first derivative of the base-state density profile is negative, the instability may develop as a stationary or as an oscillatory mode (complex eigenvalue). The neutral stability curve obtained analytically is in agreement with the earlier findings. The fact that the eigenvalues are strictly real in the context of single-species RT instabilities also follows from the work presented here.

To this end, the geometry and the governing equations are introduced in § 2, along with the base-state density profiles in the non-dimensional  $(R, \tau)$  plane. In § 3 we reduce this to a characteristic value problem from which the conditions for instability can be obtained, which is discussed in § 4. After considering some special cases, namely single-species RT instability and when  $\tau = 0$ , the paper finishes in § 5 with the main conclusions.

## 2. Geometry and governing equations

We consider a two-dimensional porous medium in which gravity points downwards and two miscible solutions are in contact along a horizontal interface such as that sketched in figure 1. The upper solution contains a solute A while the lower solution contains a solute B, with initial concentrations  $A_0$  and  $B_0$ , respectively. The  $y$ -axis is defined as the horizontal axis where the solutions are initially in contact, and the  $x$ -axis as the vertical one increasing in the downwards direction, such that  $x < 0$  is the upper region and  $x > 0$  is the lower region. By considering dilute

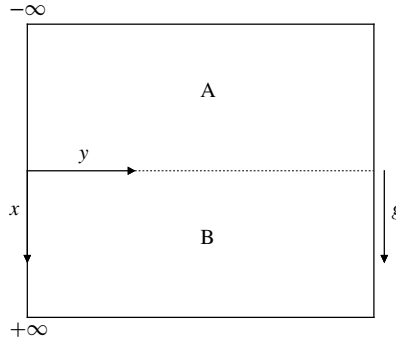


FIGURE 1. Sketch of the initial physical problem.

solutions, the diffusion coefficients  $D_A$  and  $D_B$  of species A and B, respectively, can be assumed constant. Moreover, the density varies linearly with the concentrations as  $\rho(A, B) = \rho_0[1 + \alpha_A A + \alpha_B B]$ , where  $\rho_0$  is the density of the pure solvent, A and B are the concentrations of the respective species, and  $\alpha_A$  and  $\alpha_B$  are their corresponding solutal expansion coefficients defined as  $\alpha_A = (1/\rho_0)\partial\rho/\partial A$  and  $\alpha_B = (1/\rho_0)\partial\rho/\partial B$ . The dynamics of the buoyancy-driven instabilities of this miscible interface are described by Darcy’s equation coupled to advection–diffusion equations for the concentrations A and B. The set of equations governing the system can be non-dimensionalised by considering the characteristic velocity  $\mathbb{U} = gK\alpha_A A_0/\mu$ , length  $\mathbb{L} = D_A\phi/\mathbb{U}$  and time  $\mathbb{T} = \mathbb{L}/\mathbb{U}$  scales, where  $g$  is the magnitude of the acceleration due to gravity,  $K$  is the permeability,  $\mu$  is the dynamic viscosity and  $\phi$  is the porosity (taken as 1). The resulting non-dimensional equations read (Trevelyan *et al.* 2011; Gopalakrishnan *et al.* 2018):

$$\nabla p = -\mathbf{u} + (A + RB)\hat{\mathbf{i}}_x, \tag{2.1}$$

$$\nabla \cdot \mathbf{u} = 0, \tag{2.2}$$

$$A_t + \mathbf{u} \cdot \nabla A = \nabla^2 A, \tag{2.3}$$

$$B_t + \mathbf{u} \cdot \nabla B = \tau \nabla^2 B, \tag{2.4}$$

where  $p$  is the pressure,  $\mathbf{u}$  is the flow velocity,  $\hat{\mathbf{i}}_x$  is the unit vector in the direction of gravity,  $R = \alpha_B B_0/\alpha_A A_0$  is the dimensionless buoyancy ratio and  $\tau = D_B/D_A$  is the ratio of the diffusion coefficients (Trevelyan *et al.* 2011; Gopalakrishnan *et al.* 2018). The buoyancy ratio  $R$  expresses the relative contributions of species B and A to the dimensional density profile and is also equal to  $R = (\rho_B - \rho_0)/(\rho_A - \rho_0)$ , where  $\rho_A = \rho_0(1 + \alpha_A A_0)$  and  $\rho_B = \rho_0(1 + \alpha_B B_0)$  are the densities of the upper and lower solutions, respectively. The concentrations are non-dimensionalised using  $A_0$  while the density is scaled as  $(\rho(A, B)/\rho_0 - 1)/\alpha_A A_0$ . As initial conditions, we impose in the top layer ( $x < 0$ )  $A = 1, B = 0$ , while in the bottom layer ( $x > 0$ )  $A = 0, B = 1$ , with no velocity in the entire domain ( $\mathbf{u} = \mathbf{0}$ ). The boundary conditions are  $A = 1, B = 0$  for  $x \rightarrow -\infty$ , and  $A = 0, B = 1$  for  $x \rightarrow \infty$ .

In the absence of convection, the base-state concentration profiles, assuming a domain of infinite height, are given by

$$\bar{A}(x, t) = \frac{1}{2} \operatorname{erfc} \left( \frac{x}{2\sqrt{t}} \right), \quad \bar{B}(x, t) = \frac{1}{2} \operatorname{erfc} \left( -\frac{x}{2\sqrt{\tau t}} \right), \tag{2.5a,b}$$

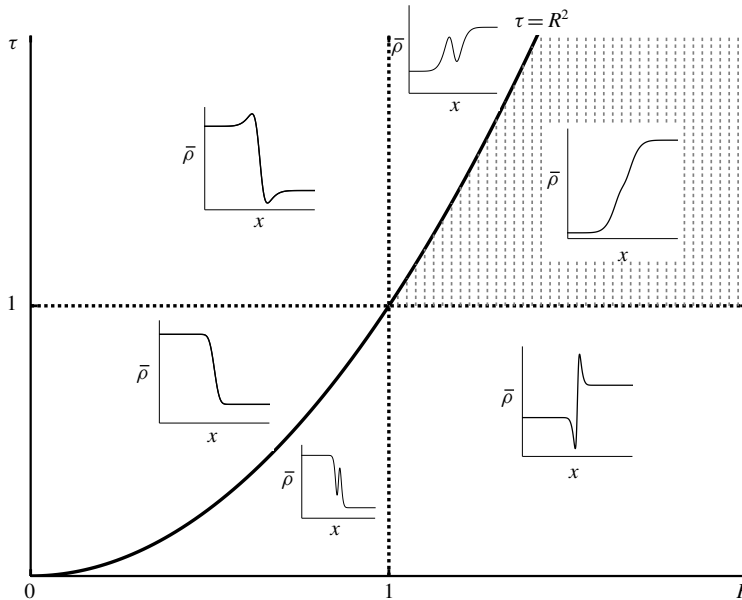


FIGURE 2. Typical base-state density profiles  $\bar{\rho}(x, t)$  in the  $(R, \tau)$  parameter space. Base-state density profiles are monotonically increasing in the shaded region.

while the non-dimensional base-state density profile can be constructed as

$$\bar{\rho}(x, t) = \bar{A}(x, t) + R\bar{B}(x, t). \tag{2.6}$$

The base state of our problem follows a diffusive dynamics satisfying (2.3) and (2.4) with  $\mathbf{u} = \mathbf{0}$  along with the initial conditions specified earlier. This is in contrast with the earlier analytical studies on the stability of buoyancy-driven flows, where linear base states were considered (Huppert & Sparks 1984; Gandhi & Trevelyan 2014). As noted in Trevelyan *et al.* (2011), the density is antisymmetric about  $x = 0$ , as  $\bar{\rho}(x, t) + \bar{\rho}(-x, t) = 1 + R$ . This also implies that the convective patterns in porous media flows evolve the same way on both sides of the initial interface (Trevelyan *et al.* 2011).

The different buoyancy-driven instabilities discussed in § 1, namely the Rayleigh–Taylor (RT), double-diffusive (DD) and diffusive-layer convection (DLC), can be obtained depending on the values of parameters  $R$  and  $\tau$ . The RT instabilities develop when  $R < 1$ , as we have a ‘heavy on top of light’ configuration; whereas for  $R > 1$ , the system is initially in a stable stratification (‘light on top of heavy’). The single-species RT instability occurs when  $\tau = 1$  and  $R < 1$ , as the diffusion coefficients are the same. When the solutes diffuse at different rates  $\tau \neq 1$ , DD and DLC mechanisms can destabilise the miscible interface. The DD instabilities are at play when  $\tau > 1$ , whereas DLC mechanisms develop over time when  $\tau < 1$ . Indeed, when  $R < 1$ , DD and DLC instabilities are coupled with RT effects. Typical base-state density profiles corresponding to RT, DD and DLC are shown in figure 2 in the  $(R, \tau)$  plane. A more complete description of the various features of the base-state density profiles pertaining to different instability mechanisms can be found in Trevelyan *et al.* (2011).

We now turn our attention to the problem at hand, i.e. to obtain the conditions for this system to be linearly unstable along with the various features of the instability, from the base-state density profiles.

3. Reduction to a characteristic value problem

As the flow is incompressible, we consider the streamfunction  $\psi$  formulation, using  $u = \psi_y$  and  $v = -\psi_x$ , where  $\mathbf{u} = (u, v)$ , thereby satisfying  $\nabla \cdot \mathbf{u} = 0$ . Taking the curl of (2.1) and substituting  $\psi$  into (2.3) and (2.4), we have the following system of equations (Trevelyan *et al.* 2011):

$$\nabla^2 \psi = A_y + RB_y, \tag{3.1}$$

$$A_t + \psi_y A_x - \psi_x A_y = \nabla^2 A, \tag{3.2}$$

$$B_t + \psi_y B_x - \psi_x B_y = \tau \nabla^2 A. \tag{3.3}$$

Introducing perturbations in the form of normal modes to the base-state solutions (which are assumed to vary more slowly than the perturbations) we have

$$[\psi, A, B] = [0, \bar{A}, \bar{B}] + \epsilon \exp(\sigma t + ik y) [ik^{-1} \hat{\psi}, \hat{A}, \hat{B}], \tag{3.4}$$

where  $\epsilon$  is a small parameter,  $k$  denotes the wavenumber and the complex frequency  $\sigma (= \sigma_r + i\sigma_i)$  is the eigenvalue. The overbars indicate base-state variables. With a positive growth rate,  $\sigma_r > 0$ , the perturbation grows exponentially in time and the system is linearly unstable. While adopting the normal mode approach to describe any arbitrary disturbance, we have made a quasi-steady-state approximation (QSSA) by assuming that the base state is varying more slowly than the perturbations (Farrell & Ioannou 1996). Although there is only one time scale in this problem,  $\mathbb{T}$ , which would imply that the base state and disturbances both evolve with this characteristic time scale, the base state under consideration here smears out diffusively in time, and hence the QSSA is justified as noted in the earlier works by Tan & Homsy (1986) and Trevelyan *et al.* (2011). Here it is pertinent to point out that another approach to the QSSA has recently been adopted in the works of Kim & Choi (2011), Pramanik & Mishra (2013) and Hota & Mishra (2018) by using a similarity transformation  $(\xi, t)$ , where  $\xi = x/\sqrt{t}$ , such that the base-state concentration profile does not explicitly depend on time, and hence can be translated along the flow direction as time passes. At a time instant near zero, such a self-similar QSSA method is shown to give more accurate results in comparison to the classical QSSA, though excellent agreement is observed for later times.

We now consider the base-state solution at a given time  $t$  and treat this frozen profile as though it were steady. Linearising system (3.1)–(3.3) in  $\epsilon$ , we obtain

$$\hat{\psi}_{xx} = k^2(\hat{\psi} + \hat{A} + R\hat{B}), \tag{3.5}$$

$$\sigma \hat{A} = \hat{A}_{xx} - k^2 \hat{A} + \bar{A}_x \hat{\psi}, \tag{3.6}$$

$$\sigma \hat{B} = \tau(\hat{B}_{xx} - k^2 \hat{B}) + \bar{B}_x \hat{\psi}. \tag{3.7}$$

If we define  $\mathcal{L} = (D^2 - k^2)$ , where  $D = d/dx$ , we have

$$\mathcal{L} \hat{\psi} = k^2(\hat{A} + R\hat{B}), \tag{3.8}$$

$$\sigma \hat{A} = \mathcal{L} \hat{A} + \bar{A}_x \hat{\psi}, \tag{3.9}$$

$$\sigma \hat{B} = \tau \mathcal{L} \hat{B} + \bar{B}_x \hat{\psi}. \tag{3.10}$$

The boundary conditions with respect to which the above equations must be solved are given by

$$|\hat{A}| = |\hat{B}| = |\hat{\psi}| = 0, \quad \text{for } x = \pm\infty, \tag{3.11}$$

as we have considered an infinite domain with the perturbations decaying at the corresponding vertical limits.

We have  $\bar{\rho} = \bar{A} + R\bar{B}$  (2.6), and consequently  $\bar{\rho}_x = \bar{A}_x + R\bar{B}_x$ . Multiplying (3.10) by  $R$  gives

$$\sigma R\hat{B} = R\tau\mathcal{L}\hat{B} + R\bar{B}_x\hat{\psi}, \tag{3.12}$$

and summing with (3.9), we get

$$\sigma\hat{A} + \sigma R\hat{B} = \mathcal{L}\hat{A} + R\tau\mathcal{L}\hat{B} + \bar{\rho}_x\hat{\psi}. \tag{3.13}$$

With  $R\hat{B} = (1/k^2)\mathcal{L}\hat{\psi} - \hat{A}$  (from (3.8)), equation (3.13) reduces to

$$\sigma\hat{A} + \sigma[(1/k^2)\mathcal{L}\hat{\psi} - \hat{A}] = \mathcal{L}\hat{A} + \tau\mathcal{L}[(1/k^2)\mathcal{L}\hat{\psi} - \hat{A}] + \bar{\rho}_x\hat{\psi}, \tag{3.14a}$$

$$\frac{\sigma}{k^2}\mathcal{L}\hat{\psi} = \mathcal{L}\hat{A} + \frac{\tau}{k^2}\mathcal{L}^2\hat{\psi} - \tau\mathcal{L}\hat{A} + \bar{\rho}_x\hat{\psi}, \tag{3.14b}$$

$$\left[\frac{\sigma}{k^2}\mathcal{L} - \frac{\tau}{k^2}\mathcal{L}^2 - \bar{\rho}_x\right]\hat{\psi} = (1 - \tau)\mathcal{L}\hat{A}, \tag{3.14c}$$

$$[\sigma\mathcal{L} - \tau\mathcal{L}^2 - \bar{\rho}_xk^2]\hat{\psi} = k^2(1 - \tau)\mathcal{L}\hat{A}. \tag{3.14d}$$

Using  $\mathcal{L}\hat{A} = \sigma\hat{A} - \bar{A}_x\hat{\psi}$  (from (3.9)), equation (3.14d) can be rewritten as

$$[\sigma\mathcal{L} - \tau\mathcal{L}^2 - \bar{\rho}_xk^2]\hat{\psi} = k^2(1 - \tau)(\sigma\hat{A} - \bar{A}_x\hat{\psi}), \tag{3.15a}$$

$$[\sigma\mathcal{L} - \tau\mathcal{L}^2 - \bar{\rho}_xk^2 + k^2(1 - \tau)\bar{A}_x]\hat{\psi} = k^2(1 - \tau)\sigma\hat{A}. \tag{3.15b}$$

Substituting the expression for  $\hat{\psi}$  from (3.9) ( $\hat{\psi} = (\sigma\hat{A} - \mathcal{L}\hat{A})/\bar{A}_x$ ) in (3.15b), we get

$$\sigma^2\mathcal{L}\hat{A} - \sigma[(1 + \tau)\mathcal{L}^2 + \bar{\rho}_xk^2]\hat{A} + \tau\mathcal{L}^3\hat{A} - k^2\zeta(x)\mathcal{L}\hat{A} = 0, \tag{3.16}$$

where  $\zeta(x) = \bar{A}_x(1 - \tau) - \bar{\rho}_x$ .

The above equation along with the boundary conditions (3.11) constitute a characteristic value problem, which is indeed a formidable one if it has to be solved in any direct manner. Fortunately, it will appear that this is not necessary to obtain the conditions for instability from the characteristics of the base-state density profile  $\bar{\rho}(x, t)$ . For this, a method based on a variational principle (Roberts 1960; Chandrasekhar 1961) can be used, which is described in the following section.

#### 4. Conditions for instability

We multiply (3.16) by  $\hat{A}^*$ , the complex conjugate of  $\hat{A}$ , and integrate over the range of  $x$ , the vertical extent of the domain, which gives

$$\int_{-\infty}^{\infty} \sigma^2\hat{A}^*\mathcal{L}\hat{A} \, dx - \int_{-\infty}^{\infty} \hat{A}^*\sigma[(1 + \tau)\mathcal{L}^2 + \bar{\rho}_xk^2]\hat{A} \, dx + \int_{-\infty}^{\infty} \hat{A}^*(\tau\mathcal{L}^3\hat{A} - k^2\zeta(x)\mathcal{L}\hat{A}) \, dx = 0. \tag{4.1}$$

It makes sense to write the above integrals, as the operator  $\mathcal{L} = (D^2 - k^2)$  is self-adjoint, implying that it is closed and bounded on  $\mathbb{R}$ , where  $\mathbb{R}$  is the extended real line.

To simplify the terms corresponding to each integral, it is convenient to define the following:

$$\mathbb{I}_1 = \int_{-\infty}^{\infty} \sigma^2\hat{A}^*\mathcal{L}\hat{A} \, dx, \tag{4.2}$$

$$\mathbb{I}_2 = \int_{-\infty}^{\infty} -\sigma \hat{A}^* [(\tau + 1)\mathcal{L}^2 + \bar{\rho}_x k^2] \hat{A} \, dx, \tag{4.3}$$

$$\mathbb{I}_3 = \int_{-\infty}^{\infty} \hat{A}^* (\tau \mathcal{L}^3 \hat{A} - k^2 \zeta(x) \mathcal{L} \hat{A}) \, dx. \tag{4.4}$$

We have  $\mathbb{I}_1$ , which can be rewritten as

$$\mathbb{I}_1 = \int_{-\infty}^{\infty} \sigma^2 \hat{A}^* (D^2 - k^2) \hat{A} \, dx \tag{4.5a}$$

$$= \int_{-\infty}^{\infty} \sigma^2 \hat{A}^* D^2 \hat{A} \, dx - \int_{-\infty}^{\infty} \sigma^2 \hat{A}^* k^2 \hat{A} \, dx \tag{4.5b}$$

$$= \sigma^2 [\hat{A}^* D \hat{A}]_{-\infty}^{\infty} - \int_{-\infty}^{\infty} D \hat{A}^* D \hat{A} \, dx - \int_{-\infty}^{\infty} \sigma^2 |k \hat{A}|^2 \, dx \tag{4.5c}$$

$$= \int_{-\infty}^{\infty} -\sigma^2 |D \hat{A}|^2 \, dx - \int_{-\infty}^{\infty} \sigma^2 |k \hat{A}|^2 \, dx \tag{4.5d}$$

$$= \int_{-\infty}^{\infty} -\sigma^2 [|D \hat{A}|^2 + |k \hat{A}|^2] \, dx, \tag{4.5e}$$

since the integrated part vanishes on account of the boundary conditions (3.11). In a similar manner the integrals corresponding to  $\mathbb{I}_2$  and  $\mathbb{I}_3$  can be simplified as (see appendix A)

$$\mathbb{I}_2 = \int_{-\infty}^{\infty} -\sigma [(\tau + 1)(D^2 - k^2) \hat{A}]^2 + \bar{\rho}_x |k \hat{A}|^2] \, dx, \tag{4.6}$$

$$\mathbb{I}_3 = \int_{-\infty}^{\infty} -\tau [|D(D^2 - k^2) \hat{A}|^2 + |k(D^2 - k^2) \hat{A}|^2] \, dx + \int_{-\infty}^{\infty} k^2 \zeta(x) [|D \hat{A}|^2 + |k \hat{A}|^2] \, dx. \tag{4.7}$$

Thus (4.1), which was broken down as  $\mathbb{I}_1$ ,  $\mathbb{I}_2$  and  $\mathbb{I}_3$ , reads as follows:

$$\begin{aligned} & \int_{-\infty}^{\infty} -\sigma^2 [|D \hat{A}|^2 + |k \hat{A}|^2] \, dx + \int_{-\infty}^{\infty} -\sigma [(\tau + 1)(D^2 - k^2) \hat{A}]^2 + \bar{\rho}_x |k \hat{A}|^2] \, dx + \dots \\ & + \int_{-\infty}^{\infty} -\tau [|D(D^2 - k^2) \hat{A}|^2 + |k(D^2 - k^2) \hat{A}|^2] \, dx + \int_{-\infty}^{\infty} k^2 \zeta(x) [|D \hat{A}|^2 + |k \hat{A}|^2] \, dx = 0. \end{aligned} \tag{4.8}$$

Thus we have

$$\int_{-\infty}^{\infty} (\sigma^2 \mathcal{X} + \sigma \mathcal{Y} + \mathcal{Z}) \, dx = 0, \tag{4.9}$$

where

$$\mathcal{X} = [|D \hat{A}|^2 + |k \hat{A}|^2], \tag{4.10}$$

$$\mathcal{Y} = [(1 + \tau)(D^2 - k^2) \hat{A}]^2 + \bar{\rho}_x |k \hat{A}|^2, \tag{4.11}$$

$$\mathcal{Z} = \tau [|D(D^2 - k^2) \hat{A}|^2 + |k(D^2 - k^2) \hat{A}|^2] - k^2 \zeta(x) [|D \hat{A}|^2 + |k \hat{A}|^2]. \tag{4.12}$$

Note that the terms  $\mathcal{X}$ ,  $\mathcal{Y}$ ,  $\mathcal{Z}$  are real, whereas  $\sigma$  may have real ( $\sigma_r$ ) and imaginary ( $\sigma_i$ ) parts. If  $\sigma_r$  is positive, then the system would have perturbations that would grow



exponentially in time, and is linearly unstable; whereas a negative  $\sigma_r$  implies that the system is linearly stable. The perturbations could be oscillatory or stationary, with a non-zero value of  $\sigma_i$  corresponding to the former, and  $\sigma_i = 0$  to the latter. We now look for the conditions for instability. Equation (4.9) reads as

$$\int_{-\infty}^{\infty} [(\sigma_r^2 - \sigma_i^2 + i2\sigma_r\sigma_i)\mathcal{X} + (\sigma_r + i\sigma_i)\mathcal{Y} + \mathcal{Z}] dx = 0. \tag{4.13}$$

Considering the imaginary part, we have

$$\left. \begin{aligned} &\int_{-\infty}^{\infty} \sigma_i(2\sigma_r\mathcal{X} + \mathcal{Y}) dx = 0, \\ &\int_{-\infty}^{\infty} \sigma_i(2\sigma_r[|D\hat{A}|^2 + |k\hat{A}|^2] + [(1 + \tau)(D^2 - k^2)\hat{A}]^2 + \bar{\rho}_x|k\hat{A}|^2) dx = 0. \end{aligned} \right\} \tag{4.14}$$

If we consider  $\sigma_i \neq 0$  (oscillatory modes), the terms in parentheses are strictly positive, with the exception of the gradient of the base-state density profile  $\bar{\rho}_x$ , which could be positive or negative or both within the domain, and  $\sigma_r$ . For instability, we know that  $\sigma_r > 0$ . This implies that there must be a region within the domain where  $\bar{\rho}_x < 0$ , which is a sufficient condition for instability.

So we have our first necessary criterion for instability with oscillatory modes: there must be a region within the domain where  $\bar{\rho}_x < 0$ . On the contrary, if  $\bar{\rho}_x$  is positive throughout the domain, then the system is uniquely unstable to stationary modes such that  $\sigma_i = 0$ .

We now look for the conditions for the flow to be unstable when  $\bar{\rho}_x$  is positive throughout the domain. Using the expression for  $\bar{\rho}$  (2.6) and differentiating with respect to  $x$ , we have the expression for  $\bar{\rho}_x$  given by

$$\bar{\rho}_x = \frac{-\exp[-x^2/4t]}{2\sqrt{\pi t}} + \frac{\exp[-x^2/4t\tau]R}{2\sqrt{\pi t\tau}}. \tag{4.15}$$

The density profiles are monotonically increasing downwards when

$$1 \leq \tau \leq R^2, \tag{4.16}$$

and  $\bar{\rho}_x$  is positive throughout the domain (the shaded region in figure 2). For these parameter settings, the system is unstable to purely real eigenvalues ( $\sigma_i = 0$ ). Using  $\sigma_i = 0$  in (4.13), we have

$$\int_{-\infty}^{\infty} (\sigma_r^2\mathcal{X} + \sigma_r\mathcal{Y} + \mathcal{Z}) dx = 0, \tag{4.17}$$

and substituting the expressions for  $\mathcal{X}$ ,  $\mathcal{Y}$  and  $\mathcal{Z}$  gives

$$\begin{aligned} &\int_{-\infty}^{\infty} (\sigma_r^2[|D\hat{A}|^2 + |k\hat{A}|^2] + \sigma_r[(1 + \tau)(D^2 - k^2)\hat{A}]^2 + \bar{\rho}_x|k\hat{A}|^2 \\ &\quad + \tau[|D(D^2 - k^2)\hat{A}|^2 + |k(D^2 - k^2)\hat{A}|^2] - k^2\zeta(x)[|D\hat{A}|^2 + |k\hat{A}|^2]) dx = 0. \end{aligned} \tag{4.18}$$

The terms corresponding to  $\mathcal{X}$  and  $\mathcal{Y}$  are strictly positive as  $\bar{\rho}_x$  is positive throughout the domain. So we now turn our attention to  $\zeta(x)$  as the remaining terms are positive. We have

$$\zeta(x) = \bar{A}_x(1 - \tau) - \bar{\rho}_x, \tag{4.19}$$

where  $\bar{A}_x$  is given by

$$\bar{A}_x = \frac{-\exp[-x^2/4t]}{2\sqrt{\pi t}}. \tag{4.20}$$

Using the above, we have

$$\zeta(x) = \frac{\exp[-x^2/4t]\tau}{2\sqrt{\pi t}} - \frac{\exp[-x^2/4t]R}{2\sqrt{\pi t}\sqrt{\tau}}. \tag{4.21}$$

The second derivative of the base-state density profile is given by

$$\bar{\rho}_{xx} = \frac{\exp[-x^2/4t]x}{4\sqrt{\pi t^{3/2}}} - \frac{\exp[-x^2/4t]Rx}{4\sqrt{\pi t^{3/2}}\tau^{3/2}}. \tag{4.22}$$

Using this, the equation for  $\zeta(x)$  simplifies as

$$\zeta(x) \frac{x}{2\tau t} = \bar{\rho}_{xx}, \tag{4.23}$$

$$\zeta(x) = \frac{2\tau t}{x} \bar{\rho}_{xx}. \tag{4.24}$$

If  $\zeta(x)$  is negative throughout the domain, from (4.18)  $\sigma_r < 0$  and the system is linearly stable. For instability,  $\zeta(x)$  must be greater than zero within some region of the domain. Thus we have that if  $\bar{\rho}_{xx} > 0$  for  $x < 0$  (above the initial interface) and if  $\bar{\rho}_{xx} < 0$  for  $x > 0$  (below the initial interface), then  $\sigma_r < 0$  and the system is linearly stable. The instability develops on either side of the interface, which implies that above the interface ( $x < 0$ ) there must be region where  $\bar{\rho}_{xx} < 0$  and, correspondingly, below the interface ( $x > 0$ ) there must be a region where  $\bar{\rho}_{xx} > 0$ . Also, it is important to note that, at  $t = 0$ ,  $\zeta(x) = 0$ , and from this it follows that  $\sigma_r < 0$ . So the flows where  $\bar{\rho}_x > 0$  throughout the domain are initially linearly stable with the instability developing in time.

The density profile has an inflection point at the interface corresponding to  $x = 0$ , as we can see from the expression (4.22) that  $\bar{\rho}_{xx} = 0$ . Instability, however, requires that  $\bar{\rho}_{xx} < 0$  above the interface ( $x < 0$ ) and  $\bar{\rho}_{xx} > 0$  below the interface ( $x > 0$ ). Since  $\bar{\rho}_x > 0$  throughout the domain, above and below the interface, there has to be an additional point such that  $\bar{\rho}_{xx} = 0$  on either side of the domain such that  $\bar{\rho}_{xx}$  goes from positive to negative above the initial interface, and from negative to positive below the interface. Otherwise it follows from (4.18) that  $\sigma_r < 0$ . Thus the boundary of stability when  $\bar{\rho}_x > 0$  throughout the domain can be obtained by using  $\bar{\rho}_{xx} = 0$  (for  $x \neq 0$ ) and is given by

$$R > \tau^{3/2} \exp \left[ \left( \frac{x^2}{4t} \right) \left( \frac{1}{\tau} - 1 \right) \right], \tag{4.25}$$

where all the eigenvalues in this regime are strictly real. The above function has a minimum value at  $x = 0$ , which gives the limiting boundary for instability beyond which the flows are linearly stable:

$$R = \tau^{3/2}. \tag{4.26}$$

The fact that all the eigenvalues are strictly real in such regimes has been numerically observed by Trevelyan *et al.* (2011, p. 52), which follows as a direct consequence from the discussion presented here. A similar asymptotic limit had been shown by

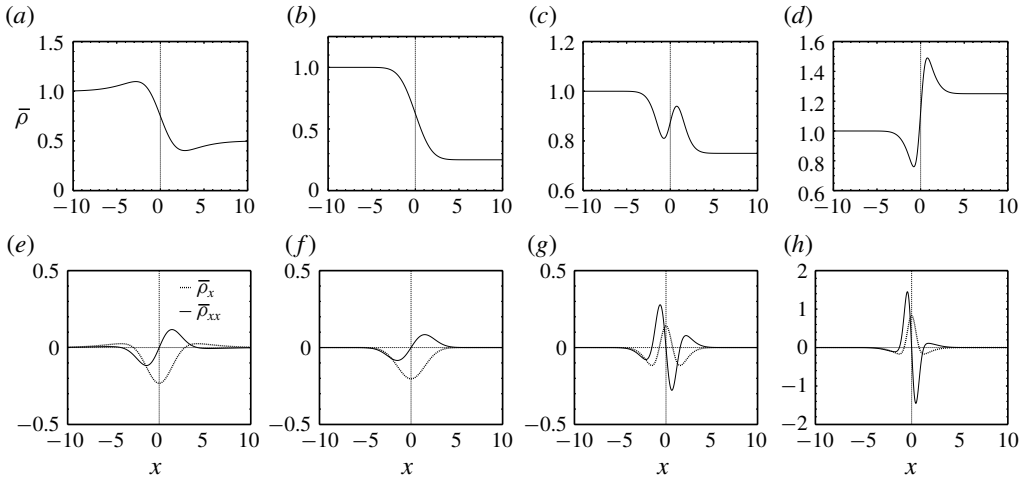


FIGURE 3. (a–d) Typical base-state density profiles  $\bar{\rho}(x, t)$  at  $t > 0$  for different combinations of  $(R, \tau)$ ; (e–h) the corresponding first derivatives  $\bar{\rho}_x(x, t)$  (dotted line) and second derivatives  $\bar{\rho}_{xx}(x, t)$  (continuous line). Parameter settings: (a,e)  $\tau = 8.0, R = 0.50$ ; (b,f)  $\tau = 0.80, R = 0.25$ ; (c,g)  $\tau = 0.25, R = 0.75$ ; and (d,h)  $\tau = 0.10, R = 1.25$ .

Huppert & Manins (1973) by considering linear base states, and is consistent with the numerical stability analysis carried out by Trevelyan *et al.* (2011). The result presented here when the density profiles are monotonically increasing downwards is qualitatively similar to the Rayleigh criterion observed in the case of shear flows (Lord Rayleigh 1880; Taylor 1915).

We shall now briefly overview the various base-state density profile configurations in the  $(R, \tau)$  plane to summarise the results. Figure 3(a–c) shows some typical base-state density profiles for  $R < 1$  (RT instability) whereas figure 3(d) corresponds to a DLC scenario. The density profiles have a region of  $x$  where  $\bar{\rho}_x < 0$ , which can be seen in figure 3(e,f) and they are linearly unstable to stationary or oscillatory disturbances. It is also interesting to note that the regions corresponding to  $\bar{\rho}_x < 0$  include the initial interface  $x = 0$  or are close to it for the scenarios corresponding to RT instabilities, which is also where the eigenfunctions are localised (Trevelyan *et al.* 2011). The second derivatives  $\bar{\rho}_{xx}$  may have both positive and negative regions on either side of the interface or could be either positive or negative, as can be seen in figure 3(e,f).

Base-state profiles that are monotonically increasing are shown in figure 4(a–d), with their corresponding  $\bar{\rho}_x$  and  $\bar{\rho}_{xx}$  in figure 4(e,f). In all these cases,  $\bar{\rho}_x > 0$  throughout the domain. In figure 4(e,f) we can see that for  $x < 0$  there is a region where  $\bar{\rho}_{xx} < 0$  and a region where  $\bar{\rho}_{xx} > 0$  for  $x > 0$ , or in other words  $\bar{\rho}_{xx} = 0$  at some location on either side of the interface. In such regimes, maximum growth rates are real and instability arises as stationary modes. A case corresponding to the asymptotic stability limit is shown in figure 4(g) beyond which  $\bar{\rho}_{xx} > 0$  above the initial interface and  $\bar{\rho}_{xx} < 0$  below (see figure 4h).

#### 4.1. Single-species RT instability

The single-species RT instability has recently received renewed attention due to its potential role in geological carbon dioxide storage (Huppert & Neufeld 2014; Slim

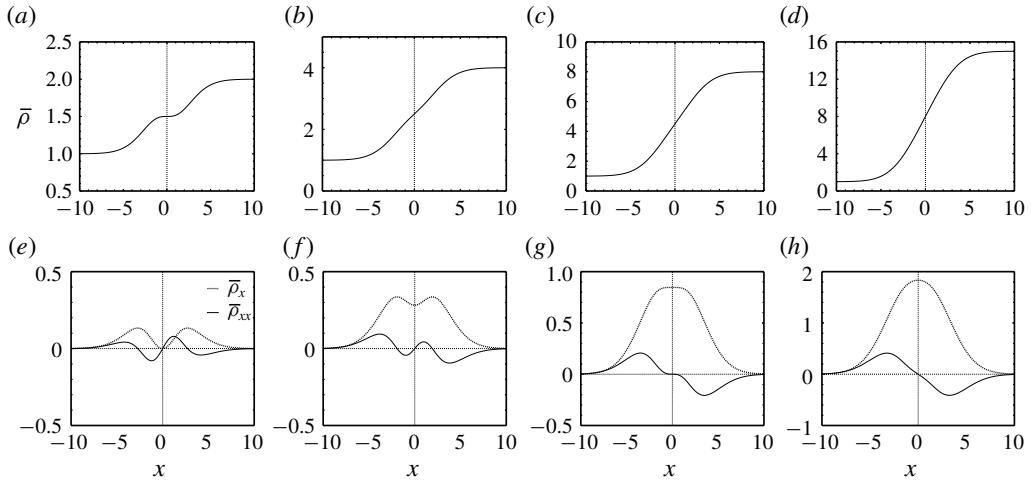


FIGURE 4. (a–d) Base-state density profiles that are monotonically increasing; (e–h) corresponding  $\bar{\rho}_x(x, t)$  (dotted line) and  $\bar{\rho}_{xx}(x, t)$  (continuous line). Parameter settings:  $\tau = 4$  and (a,e)  $R = 2.0$ , (b,f)  $R = 4.0$ , (c,g)  $R = 8.0$ , and (d,h)  $R = 15.0$ .

2014; Sardina *et al.* 2018; De Paoli *et al.* 2019a). Here we shall briefly discuss the special case of a single-species system that amounts to considering  $\tau = 1$ . We have from (3.14d)

$$\left[ \frac{\sigma}{k^2} \mathcal{L} - \frac{1}{k^2} \mathcal{L}^2 - \bar{\rho}_x \right] \hat{\psi} = 0. \tag{4.27}$$

The above can be rewritten as

$$-\sigma(D^2 - k^2)\hat{\psi} + (D^2 - k^2)^2\hat{\psi} = -\bar{\rho}_x k^2 \hat{\psi} \tag{4.28}$$

because  $\mathcal{L} = (D^2 - k^2)$ . We have

$$(D^2 - k^2)(D^2 - k^2 - \sigma)\hat{\psi} = -\bar{\rho}_x k^2 \hat{\psi}. \tag{4.29}$$

Letting  $(D^2 - k^2)\hat{\psi} = \mathcal{G}$  we rewrite the above equation as

$$(D^2 - k^2 - \sigma)\mathcal{G} = -\bar{\rho}_x k^2 \hat{\psi}. \tag{4.30}$$

Multiplying the above equation by  $\hat{\psi}^*$  (the complex conjugate of  $\hat{\psi}$ ) and integrating over the range of  $x$  (the vertical extent of the domain) we get

$$\int_{-\infty}^{\infty} \hat{\psi}^* (D^2 - k^2 - \sigma)\mathcal{G} \, dx = - \int_{-\infty}^{\infty} \hat{\psi}^* \bar{\rho}_x k^2 \hat{\psi} \, dx. \tag{4.31}$$

Considering the left-hand side of (4.31) we have

$$\int_{-\infty}^{\infty} \hat{\psi}^* (D^2 - k^2 - \sigma)\mathcal{G} \, dx = \int_{-\infty}^{\infty} \hat{\psi}^* (D^2 - k^2)\mathcal{G} \, dx - \int_{-\infty}^{\infty} \sigma \hat{\psi}^* \mathcal{G} \, dx. \tag{4.32}$$

As  $\mathcal{G} = (D^2 - k^2)\hat{\psi}$ , equation (4.32) simplifies to

$$\int_{-\infty}^{\infty} |\mathcal{G}|^2 \, dx - \int_{-\infty}^{\infty} \sigma \hat{\psi}^* (D^2 - k^2)\hat{\psi} \, dx$$

$$= \int_{-\infty}^{\infty} |\mathcal{G}|^2 dx - \int_{-\infty}^{\infty} \sigma \hat{\psi}^* D^2 \hat{\psi} dx + \int_{-\infty}^{\infty} \sigma \hat{\psi}^* \hat{\psi} k^2 dx. \tag{4.33}$$

Using this in (4.31) gives

$$\int_{-\infty}^{\infty} [|\mathcal{G}|^2 + \sigma (|D\hat{\psi}|^2 + k^2|\hat{\psi}|^2)] dx + k^2 \int_{-\infty}^{\infty} \bar{\rho}_x |\hat{\psi}|^2 dx = 0. \tag{4.34}$$

The real and imaginary parts of this equation must vanish separately; and the vanishing of the imaginary part gives

$$\sigma_i \int_{-\infty}^{\infty} [|D\hat{\psi}|^2 + k^2|\hat{\psi}|^2] dx = 0, \tag{4.35}$$

where  $\sigma = \sigma_r + i\sigma_i$ . But the quantity inside the brackets is positive definite. Hence

$$\sigma_i = 0. \tag{4.36}$$

This establishes that  $\sigma$  is real. So we have

$$\int_{-\infty}^{\infty} [|\mathcal{G}|^2 + \sigma_r (|D\hat{\psi}|^2 + k^2|\hat{\psi}|^2)] dx + k^2 \int_{-\infty}^{\infty} \bar{\rho}_x |\hat{\psi}|^2 dx = 0, \tag{4.37}$$

$$\sigma_r = \frac{-k^2 \int_{-\infty}^{\infty} \bar{\rho}_x |\hat{\psi}|^2 dx - |\mathcal{G}|^2 dx}{\int_{-\infty}^{\infty} (|D\hat{\psi}|^2 + k^2|\hat{\psi}|^2) dx}. \tag{4.38}$$

From the above, we can see that, if  $\bar{\rho}_x$  is positive throughout the domain, then  $\sigma_r < 0$  and the flow is linearly stable. Only when there is a region in the base flow profile where  $\bar{\rho}_x$  is negative, can we have  $\sigma_r > 0$ , which is a necessary and sufficient condition for instability in single-species RT flows. Also, the eigenvalues are real and instability arises as non-oscillatory modes. In these flows, the onset of instability is marked by a transition from the background state to another steady state with the principle of exchange of stabilities being valid, which holds if all non-decaying disturbances are non-oscillatory in time (Chandrasekhar 1961; Davis 1969). It is also interesting to note that Rayleigh–Bénard convection and Taylor–Couette flow are two other well-known problems in which  $\sigma$  is real (Chandrasekhar 1961; Davis 1969).

#### 4.2. *Immobile species B: $\tau = 0$*

We discuss the case  $\tau = 0$ , which physically corresponds to an immobile species B. It also provides a good approximation to the case when A diffuses much faster than B. For  $\tau = 0$  from (4.14) we have

$$\int_{-\infty}^{\infty} \sigma_i (2\sigma_r [|D\hat{A}|^2 + |k\hat{A}|^2] + [(D^2 - k^2)\hat{A}]^2 + \bar{\rho}_x |k\hat{A}|^2) dx = 0. \tag{4.39}$$

As noted earlier, if  $\bar{\rho}_x$  is positive throughout the domain, then the system could be unstable only to purely real eigenvalues with  $\sigma_i = 0$ . Otherwise, they could be complex,

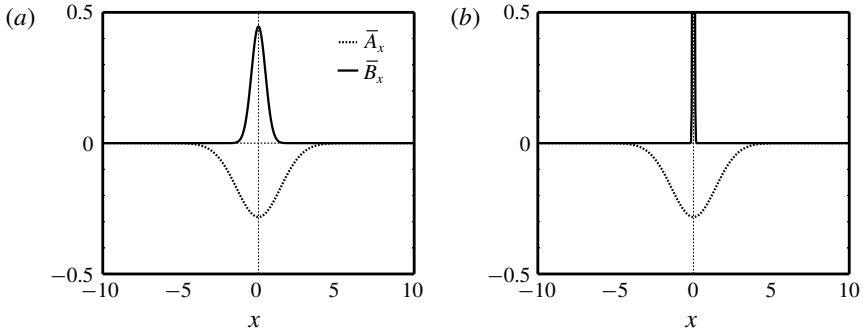


FIGURE 5. Plots of (a,b)  $\bar{A}_x$  (dotted line) and  $\bar{B}_x$  (continuous line) at  $t > 0$  for  $R = 0.50$ . Parameter settings: (a)  $\tau = 0.10$ , and (b)  $\tau = 0.001$ .

and oscillatory instabilities may be present. From (4.15) we can obtain the limit of  $R$  above which  $\bar{\rho}_x$  is strictly positive, which is given by

$$R_c = \exp \left[ -\frac{x^2}{4t} \left( 1 - \frac{1}{\tau} \right) \right] \sqrt{\tau}. \tag{4.40}$$

The gradient at  $x = 0$  is given by

$$\bar{\rho}_x|_{x=0} = \frac{1}{2\sqrt{\pi t}} \left( \frac{R}{\sqrt{\tau}} - 1 \right), \tag{4.41}$$

which indicates that, as  $\tau \rightarrow 0$ , the function goes to  $\infty$  at  $x = 0$ . When  $\tau \rightarrow 0$ ,  $\bar{B}_x = \exp[-x^2/4t\tau]/(2\sqrt{\pi t\tau})$ , and can be treated as a Dirac delta function  $\delta(x)$  as

$$\bar{B}_x = \bar{B}_x[\delta(x)\delta_{\delta,0} + (1 - \delta_{\delta,0})], \tag{4.42}$$

where  $\delta_{\delta,0}$  is the Kronecker delta. We have  $\bar{B}_x\delta(x)$  when  $\tau = 0$ , and  $\bar{B}_x$  for  $\tau \neq 0$ . So (4.39) reads as

$$\int_{-\infty}^{\infty} \sigma_i(2\sigma_r[|D\hat{A}|^2 + |k\hat{A}|^2] + [(D^2 - k^2)\hat{A}]^2 + [\bar{A}_x + R\bar{B}_x[\delta(x)\delta_{\delta,0} + (1 - \delta_{\delta,0})]]|k\hat{A}|^2) dx = 0. \tag{4.43}$$

For  $\tau = 0$  we have

$$\int_{-\infty}^{\infty} \sigma_i(2\sigma_r[|D\hat{A}|^2 + |k\hat{A}|^2] + [(D^2 - k^2)\hat{A}]^2 + [\bar{A}_x + R\bar{B}_x\delta(x)]|k\hat{A}|^2) dx = 0. \tag{4.44}$$

As  $\bar{A}_x < 0$  throughout the domain (4.20), the system could be unstable to both stationary or oscillatory disturbances. Some representative profiles of  $\bar{A}_x$  and  $\bar{B}_x$  illustrating  $\tau \rightarrow 0$  are shown in figure 5.

### 4.3. Discussion

In this section, we briefly discuss some of the implications of the results obtained in this study in the context of porous media flows. For the scenarios corresponding

to a single-species system ( $\tau = 1$ ), and in the double-diffusive regime where density profiles are monotonically increasing downwards ( $1 \leq \tau \leq R^2$ ), the instability arises as stationary modes. Whereas in the remaining ( $R, \tau$ ) parameter space bounded by the curve  $R = \tau^{3/2}$ , both stationary and oscillatory modes may destabilise the system. Oscillatory instabilities generally occur when the density gradients are altered due to both energy and mass transfer across a fluid layer provided both the mechanisms work in opposition: one of the gradients must induce a stabilising effect and the other must encourage instability. For instance, the presence of such oscillatory modes can influence the solidification process of a binary mixture where a porous mushy layer is formed via double-diffusive effects (Chen, Lu & Yang 1994; Anderson & Worster 1996). The fact that the instability arises as stationary modes in the double-diffusive regime where the base-state density profiles are monotonically increasing downwards such that the density gradient is positive throughout the domain may in turn be used in such solidification processes where oscillatory instabilities are non-desirable.

The density profiles in porous media systems may also be altered due to changes in temperature and composition as a result of chemical reactions (De Wit 2020). In the present study, as the stability boundary and the nature of instabilities were determined based on the characteristics of the density profile, the obtained results may be used in the context of buoyancy-driven instabilities in reactive systems. Such chemohydrodynamic flows may be used to tune the spatiotemporal distribution of the species, thereby providing control over pattern formation in these systems.

## 5. Concluding remarks

The interface separating two miscible solutions containing different species in porous media and Hele-Shaw cells can destabilise in the gravity field due to an unstable density stratification, or due to differential diffusion of the species. The goal of this study was to obtain the conditions for buoyancy-driven instabilities to arise from the base-state density profiles using analytical methods. If there is an interval in the spatial domain where the first derivative of the base-state density profile is negative ( $\partial \bar{\rho} / \partial x < 0$ ), the flows are linearly unstable to stationary or oscillatory disturbances. This is a sufficient condition for instability in these flows. When the base-state density profiles are strictly monotonically increasing downwards ( $1 \leq \tau \leq R^2$ , where  $R$  is the buoyancy ratio and  $\tau$  is the diffusion coefficient ratio), with the first derivative of the density profile positive throughout the domain, instability develops if and only if the second derivative changes its sign on either side of the initial interface, or alternatively there is a point where the second derivative of the base-state density profile is zero on either side of the initial interface. In such regimes the system is unstable to uniquely stationary disturbances (purely real growth rates). This is a necessary and sufficient condition for instability when the first derivative of the base-state density profile is positive throughout the domain. A necessary condition for oscillatory instabilities in these flows is that there is an interval in the spatial domain where the first derivative of the base-state density profile is negative. The asymptotic neutral stability curve ( $R = \tau^{3/2}$ ) obtained in this analysis is consistent with earlier studies where linear constant base-state profiles were used, and with numerical linear stability analyses. The fact that single-species RT instabilities arise as stationary modes also follows from the study presented in this paper. The analysis could be extended to another member of the buoyancy-driven instabilities in porous media, namely the viscous fingering instability, which is being currently investigated by the author.

**Acknowledgements**

The author would like to thank Dr A. De Wit and Dr B. Knaepen for stimulating discussions at the beginning of this work. A special word of gratitude goes to Dr A. Ranjbar for insightful feedback on some of the tools used in this study. The author gratefully acknowledges the constructive feedback from the anonymous referees during the reviewing process, which greatly helped in improving the manuscript.

**Declaration of interests**

The author reports no conflict of interest.

**Appendix A. Reduction of the integrals  $\mathbb{I}_2$  and  $\mathbb{I}_3$**

The expression for  $\mathbb{I}_2$  reads as

$$\mathbb{I}_2 = \int_{-\infty}^{\infty} -\sigma \hat{A}^* [(\tau + 1)\mathcal{L}^2 + \bar{\rho}_x k^2] \hat{A} \, dx \tag{A 1}$$

$$= \int_{-\infty}^{\infty} -\sigma \hat{A}^* (\tau + 1)(D^2 - k^2)^2 \hat{A} \, dx - \int_{-\infty}^{\infty} \sigma \hat{A}^* \bar{\rho}_x k^2 \hat{A} \, dx. \tag{A 2}$$

The first of the two integrals on the right-hand side of (A 2) can be simplified as

$$\begin{aligned} & \int_{-\infty}^{\infty} -\sigma (\tau + 1) \hat{A}^* (D^2 - k^2)^2 \hat{A} \, dx \\ &= \int_{-\infty}^{\infty} -\sigma (\tau + 1) \hat{A}^* (D^2 - k^2) (D^2 - k^2) \hat{A} \, dx \\ &= \int_{-\infty}^{\infty} -\sigma (\tau + 1) \hat{A}^* D^2 [(D^2 - k^2) \hat{A}] \, dx + \int_{-\infty}^{\infty} \sigma (\tau + 1) k^2 \hat{A}^* (D^2 - k^2) \hat{A} \, dx \\ &= -\sigma (\tau + 1) \left[ \int_{-\infty}^{\infty} \hat{A}^* D^2 [(D^2 - k^2) \hat{A}] \, dx - k^2 \int_{-\infty}^{\infty} \hat{A}^* (D^2 - k^2) \hat{A} \, dx \right]. \end{aligned} \tag{A 3}$$

After two successive integrations by parts, the first of the two integrals on the right-hand side of the foregoing equation becomes

$$\begin{aligned} \int_{-\infty}^{\infty} \hat{A}^* D^2 [(D^2 - k^2) \hat{A}] \, dx &= [\hat{A}^* D [(D^2 - k^2) \hat{A}]]_{-\infty}^{\infty} - \int_{-\infty}^{\infty} D \hat{A}^* D [(D^2 - k^2) \hat{A}] \, dx \\ &= - \left( [D \hat{A}^* [(D^2 - k^2) \hat{A}]]_{-\infty}^{\infty} - \int_{-\infty}^{\infty} D^2 \hat{A}^* [(D^2 - k^2) \hat{A}] \, dx \right) \\ &= \int_{-\infty}^{\infty} D^2 \hat{A}^* [(D^2 - k^2) \hat{A}] \, dx, \end{aligned} \tag{A 4}$$

with the integrated part vanishing on account of the boundary conditions (3.11). Using the above expression in (A 3) we get

$$\begin{aligned} & \int_{-\infty}^{\infty} -\sigma (\tau + 1) \hat{A}^* (D^2 - k^2)^2 \hat{A} \, dx \\ &= -\sigma (\tau + 1) \left[ \int_{-\infty}^{\infty} D^2 \hat{A}^* [(D^2 - k^2) \hat{A}] \, dx - \dots - k^2 \int_{-\infty}^{\infty} \hat{A}^* (D^2 - k^2) \hat{A} \, dx \right] \\ &= -\sigma (\tau + 1) \int_{-\infty}^{\infty} [(D^2 - k^2) \hat{A}]^2 \, dx. \end{aligned} \tag{A 5}$$



So expression  $\mathbb{I}_2$  reads as

$$\mathbb{I}_2 = \int_{-\infty}^{\infty} -\sigma[(\tau + 1)(D^2 - k^2)\hat{A}]^2 + \bar{\rho}_x |k\hat{A}|^2 dx. \tag{A 6}$$

Considering next  $\mathbb{I}_3$  (4.4) we have

$$\mathbb{I}_3 = \int_{-\infty}^{\infty} \hat{A}^*(\tau \mathcal{L}^3 \hat{A} - k^2 \zeta(x) \mathcal{L} \hat{A}) dx \tag{A 7}$$

$$= \int_{-\infty}^{\infty} \hat{A}^*(\tau [D^2 - k^2]^2 [D^2 - k^2] \hat{A} - k^2 \zeta(x) (D^2 - k^2) \hat{A}) dx \tag{A 8}$$

$$= \int_{-\infty}^{\infty} \hat{A}^* \tau (D^2 - k^2)^2 (D^2 - k^2) \hat{A} dx - \int_{-\infty}^{\infty} \hat{A}^* k^2 (D^2 - k^2) \zeta(x) \hat{A} dx. \tag{A 9}$$

Let the two integrals in the above equation on the right-hand side be  $\mathbb{I}_{3a}$  and  $\mathbb{I}_{3b}$ , respectively. From the first integral we have

$$\mathbb{I}_{3a} = \int_{-\infty}^{\infty} \tau \hat{A}^* (D^2 - k^2)^2 (D^2 - k^2) \hat{A} dx \tag{A 10}$$

$$= \int_{-\infty}^{\infty} \tau \hat{A}^* [(D^2 - k^2)^2] D^2 \hat{A} dx - \int_{-\infty}^{\infty} \tau k^2 \hat{A}^* (D^2 - k^2)^2 \hat{A} dx. \tag{A 11}$$

Simplifying the first integral on the right-hand side by successive integrations by parts we have

$$\begin{aligned} & \int_{-\infty}^{\infty} \tau \hat{A}^* [(D^2 - k^2)]^2 D^2 \hat{A} dx \\ &= \int_{-\infty}^{\infty} \tau \hat{A}^* D^2 (D^2 - k^2)^2 \hat{A} dx \end{aligned} \tag{A 12}$$

$$= [\tau \hat{A}^* D (D^2 - k^2)^2 \hat{A}]_{-\infty}^{\infty} - \int_{-\infty}^{\infty} \tau D \hat{A}^* D (D^2 - k^2)^2 \hat{A} dx \tag{A 13}$$

$$= - \left( [\tau D \hat{A}^* (D^2 - k^2)^2 \hat{A}]_{-\infty}^{\infty} - \int_{-\infty}^{\infty} \tau D^2 \hat{A}^* (D^2 - k^2)^2 \hat{A} dx \right) \tag{A 14}$$

$$= \int_{-\infty}^{\infty} \tau D^2 \hat{A}^* (D^2 - k^2)^2 \hat{A} dx. \tag{A 15}$$

The expression  $\mathbb{I}_{3a}$  reads as

$$\mathbb{I}_{3a} = \int_{-\infty}^{\infty} \tau D^2 \hat{A}^* (D^2 - k^2)^2 \hat{A} dx - \int_{-\infty}^{\infty} \tau k^2 \hat{A}^* (D^2 - k^2)^2 \hat{A} dx \tag{A 16}$$

$$= \int_{-\infty}^{\infty} \tau (D^2 - k^2) \hat{A}^* (D^2 - k^2)^2 \hat{A} dx. \tag{A 17}$$

Let  $\hat{W} = (D^2 - k^2) \hat{A}$ . The complex conjugate of  $\hat{W}$  is given by  $\hat{W}^* = (D^2 - k^2) \hat{A}^*$ . The expression  $\mathbb{I}_{3a}$  can be rewritten and simplified as

$$\mathbb{I}_{3a} = \int_{-\infty}^{\infty} \tau \hat{W}^* (D^2 - k^2) \hat{W} dx \tag{A 18}$$

$$= \int_{-\infty}^{\infty} \tau \hat{W}^* D^2 \hat{W} \, dx - \int_{-\infty}^{\infty} \tau k^2 \hat{W}^* \hat{W} \, dx \quad (\text{A } 19)$$

$$= \int_{-\infty}^{\infty} -\tau |D\hat{W}|^2 \, dx - \int_{-\infty}^{\infty} \tau |k\hat{W}|^2 \, dx \quad (\text{A } 20)$$

$$= \int_{-\infty}^{\infty} -\tau [|D\hat{W}|^2 + |k\hat{W}|^2] \, dx \quad (\text{A } 21)$$

$$= \int_{-\infty}^{\infty} -\tau [|D(D^2 - k^2)\hat{A}|^2 + |k(D^2 - k^2)\hat{A}|^2] \, dx. \quad (\text{A } 22)$$

We now turn our attention to  $\mathbb{I}_{3b}$ , which can be transformed in the manner

$$\mathbb{I}_{3b} = - \int_{-\infty}^{\infty} \hat{A}^* k^2 (D^2 - k^2) \zeta(x) \hat{A} \, dx \quad (\text{A } 23)$$

$$= - \int_{-\infty}^{\infty} k^2 \zeta(x) \hat{A}^* D^2 \hat{A} \, dx + \int_{-\infty}^{\infty} k^4 \zeta(x) \hat{A}^* \hat{A} \, dx \quad (\text{A } 24)$$

$$= \int_{-\infty}^{\infty} k^2 \zeta(x) |D\hat{A}|^2 \, dx + \int_{-\infty}^{\infty} \zeta(x) k^4 |\hat{A}|^2 \, dx \quad (\text{A } 25)$$

$$= \int_{-\infty}^{\infty} k^2 \zeta(x) [|D\hat{A}|^2 + |k\hat{A}|^2] \, dx. \quad (\text{A } 26)$$

So  $\mathbb{I}_3$  is given by

$$\mathbb{I}_3 = \int_{-\infty}^{\infty} -\tau [|D(D^2 - k^2)\hat{A}|^2 + |k(D^2 - k^2)\hat{A}|^2] \, dx + \int_{-\infty}^{\infty} k^2 \zeta(x) [|D\hat{A}|^2 + |k\hat{A}|^2] \, dx. \quad (\text{A } 27)$$

## REFERENCES

- ANDERSON, D. M. & WORSTER, M. G. 1996 A new oscillatory instability in a mushy layer during the solidification of binary alloys. *J. Fluid Mech.* **307**, 245–267.
- CARBALLIDO-LANDEIRA, J., TREVELYAN, P. M. J., ALMARCHA, C. & DE WIT, A. 2013 Mixed-mode instability of a miscible interface due to coupling between Rayleigh–Taylor and double-diffusive convective modes. *Phys. Fluids* **25**, 024107.
- CHANDRASEKHAR, S. 1961 *Hydrodynamic and Hydromagnetic Stability*. Clarendon.
- CHEN, F., LU, J. W. & YANG, T. L. 1994 Convective instability in ammonium chloride solution directionally solidified from below. *J. Fluid Mech.* **276**, 163–187.
- COOPER, C. A., GLASS, R. J. & TYLER, S. W. 1997 Experimental investigation of the stability boundary for double-diffusive finger convection in a Hele-Shaw cell. *Water Resour. Res.* **33**, 517–526.
- DAVIS, S. H. 1969 On the principle of exchange of stabilities. *Proc. R. Soc. Lond. A* **310**, 341–358.
- DE PAOLI, M., GIURGIU, V., ZONTA, F. & SOLDATI, A. 2019a Universal behavior of scalar dissipation rate in confined porous media. *Phys. Rev. F* **4**, 101501.
- DE PAOLI, M., ZONTA, F. & SOLDATI, A. 2019b Rayleigh–Taylor convective dissolution in confined porous media. *Phys. Rev. F* **4**, 023502.
- DE WIT, A. 2020 Chemo-hydrodynamic patterns and instabilities. *Annu. Rev. Fluid Mech.* **52**, 531–555.
- FARRELL, B. F. & IOANNOU, P. J. 1996 Generalized stability theory. Part II. Non-autonomous operators. *Oper. J. Atmos. Sci.* **53**, 2041–2053.

- FERNANDEZ, J., KUROWSKI, P., LIMAT, L. & PETITJEANS, P. 2001 Wavelength selection of fingering instability inside Hele-Shaw cells. *Phys. Fluids* **13**, 3120–3125.
- FERNANDEZ, J., KUROWSKI, P., PETITJEANS, P. & MEIBURG, E. 2002 Density-driven unstable flows of miscible fluids in a Hele-Shaw cell. *J. Fluid Mech.* **451**, 239–260.
- GANDHI, J. & TREVELYAN, P. M. J. 2014 Onset conditions for a Rayleigh–Taylor instability with step function density profiles. *J. Engng Maths* **86**, 31–48.
- GOPALAKRISHNAN, S. S., CARBALLIDO-LANDEIRA, J., DE WIT, A. & KNAEPEN, B. 2017 Relative role of convective and diffusive mixing in the miscible Rayleigh–Taylor instability in porous media. *Phys. Rev. F* **2**, 012501.
- GOPALAKRISHNAN, S. S., CARBALLIDO-LANDEIRA, J., KNAEPEN, B. & DE WIT, A. 2018 Control of Rayleigh–Taylor instability onset time and convective velocity by differential diffusion effects. *Phys. Rev. E* **98**, 011101(R).
- GREEN, T. 1984 Scales for double-diffusive fingering in porous media. *Water Resour. Res.* **20**, 1225–1229.
- GRIFFITHS, R. W. 1981 Layered double-diffusive convection in porous media. *J. Fluid Mech.* **102**, 221–248.
- HOMSY, G. M. 1987 Viscous fingering in porous media. *Annu. Rev. Fluid Mech.* **19**, 271–311.
- HOTA, T. K. & MISHRA, M. 2018 Non-modal stability analysis of miscible viscous fingering with non-monotonic viscosity profiles. *J. Fluid Mech.* **856**, 552–579.
- HUPPERT, H. E. & MANINS, P. C. 1973 Limiting conditions for salt-fingering at an interface. *Deep-Sea Res.* **20**, 315–323.
- HUPPERT, H. E. & NEUFELD, J. A. 2014 The fluid mechanics of carbon dioxide sequestration. *Annu. Rev. Fluid Mech.* **46**, 255–272.
- HUPPERT, H. E. & SPARKS, R. S. J. 1984 Double-diffusive convection due to crystallization in magmas. *Annu. Rev. Fluid Mech.* **12**, 11–37.
- HUPPERT, H. E. & TURNER, J. S. 1981 Double-diffusive convection. *J. Fluid Mech.* **106**, 299–329.
- KIM, M. C. & CHOI, C. K. 2011 The stability of miscible displacement in porous media: nonmonotonic viscosity profiles. *Phys. Fluids* **23**, 084105.
- MANICKAM, O. & HOMSY, G. M. 1995 Fingering instabilities in vertical miscible displacement flows in porous media. *J. Fluid Mech.* **288**, 75–102.
- MARTIN, J., RAKOTOMALA, N. & SALIN, D. 2002 Gravitational instability of miscible fluids in a Hele-Shaw cell. *Phys. Fluids* **14**, 902–905.
- PHILIP, J. R. 1970 Flow in porous media. *Annu. Rev. Fluid Mech.* **2**, 177–204.
- PRAMANIK, S. & MISHRA, M. 2013 Linear stability analysis of Korteweg stresses effect on miscible viscous fingering in porous media. *Phys. Fluids* **25**, 074104.
- PRINGLE, S. E. & GLASS, R. J. 2002 Double-diffusive finger convection: influence of concentration at fixed buoyancy ratio. *J. Fluid Mech.* **462**, 161–183.
- RADKO, T. 2013 *Double Diffusive Convection*. Cambridge University Press.
- RAYLEIGH, LORD 1880 On the stability or instability of certain fluid motions. *Proc. Lond. Math. Soc.* **11**, 57–70.
- ROBERTS, P. H. 1960 Characteristic value problems posed by differential equations arising in hydrodynamics and hydromagnetics. *J. Math. Anal. Appl.* **1**, 195–214.
- SAFFMAN, P. & TAYLOR, G. 1958 The penetration of a fluid into a porous medium or Hele-Shaw cell containing a more viscous liquid. *Proc. R. Soc. Lond. A* **245**, 312–329.
- SARDINA, G., BRANDT, L., BOFFETTA, G. & MAZZINO, A. 2018 Buoyancy-driven flow through a bed of solid particles produces a new form of Rayleigh–Taylor turbulence. *Phys. Rev. Lett.* **121** (22), 224501.
- SCHMITT, R. W. 1994 Double diffusion in oceanography. *Annu. Rev. Fluid Mech.* **26**, 255–285.
- SCHMITT, R. W., LEDWELL, J. R., MONTGOMERY, E. T., POLZIN, K. L. & TOOLE, J. M. 2005 Enhanced diapycnal mixing by salt fingers in the thermocline of the tropical Atlantic. *Science* **308**, 685–688.
- SLIM, A. C. 2014 Solutal-convection regimes in a two-dimensional porous medium. *J. Fluid Mech.* **741**, 461–491.

- TAN, C. T. & HOMSY, G. M. 1986 Stability of miscible displacements in porous media: rectilinear flow. *Phys. Fluids* **29**, 3549.
- TAYLOR, G. I. 1915 Eddy motion in the atmosphere. *Phil. Trans. R. Soc.* **215**, 1–26.
- TREVELYAN, P. M. J., ALMARCHA, C. & DE WIT, A. 2011 Buoyancy-driven instabilities of miscible two-layer stratifications in porous media and Hele-Shaw cells. *J. Fluid Mech.* **670**, 38–65.
- TURNER, J. S. 1979 *Buoyancy Effects in Fluids*. Cambridge University Press.
- TURNER, J. S. 1985 Multicomponent convection. *Annu. Rev. Fluid Mech.* **17**, 11–44.
- TURNER, J. S. & STOMMEL, H. 1964 A new case of convection in the presence of combined vertical salinity and temperature gradients. *Proc. Natl Acad. Sci. USA* **52**, 49–53.